ACS OMEGA

Open Access

http://pubs.acs.org/journal/acsodf

Article

A Numerical Study of Fault Reactivation Mechanisms in CO_2 Storage

Ali Mortazavi* and Torekeldi Maratov

Cite This: *ACS Omega* 2024, 9, 32513−32524

Read Online

ACCESS | Metrics & More | Article Recommendations

ABSTRACT: Due to extensive industrialization and ongoing fossil fuel consumption, CO_2 emissions have significantly contributed to climate change and rising greenhouse gas levels. The collection and storage of CO_2 in subsurface geological formations have been proposed as a feasible alternative. The well-documented In Salah storage site is the subject of the chosen case study. For the numerical analysis, a two-dimensional finite element simulation of fault reactivation processes was conducted in the context of the CO_2 storage. The goal of this research is to conduct a mechanistic numerical analysis of a typical CO_2 storage condition. The selected analysis domain is 4 km (width) × 2 km (depth) and includes all important domains and formations (overburden, main caprock, lower caprock, and underburden) of the In Salah site. The simulation results indicate that the influence of fault reactivation under 32 MPa of base injection pressure results in peak vertical deformation of 0.044 m in the caprock and a vertical displacement magnitude of 0.015−0.020 m at the surface level (Z = 0 m). The derived vertical deformation findings at the surface level are in agreement with the data obtained from the in situ InSAR monitoring system in 2009. The effects of the changes in the fault dip angle, key caprock mechanical parameters, and in situ stress ratio on the displacement profile are evaluated within the parametric study. In comparison to the benchmark numerical run, the scenario ratio of k = 0.5 led to a significant reduction in the displacement. The simulation in which the fault dip angle was 30° produced a more pessimistic result with a larger displacement field. This could be an indication of heightened fault reactivation risks associated with low-angle faults in storage sites with strong horizontal stress regimes due to the combined effect of increased shear stress and reduced inherent frictional resistance on the fault plane. Considering that a vertical fault dip angle (90°) and an additional three 20 m long vertical fractures above the reservoir produced similar vertical displacement observed with the fault dipping at a 60° angle, this indicated that the vertical faults in the vicinity of the storage site pose limited safety risks to the integrity of the sealing rock.

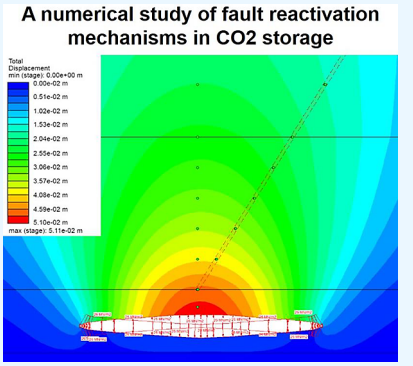

1. INTRODUCTION

Carbon dioxide (CO_2) emissions have significantly contributed to climate change and the intensified greenhouse gas effect as a result of the massive scale of industrialization and ongoing use of fossil fuels around the globe. Extensive research efforts are being made to find an effective way of regulating and reducing CO_2 emission levels in response to growing public concern over additional issues related to the rising warming effect. In light of these challenges, CO_2 capture and underground storage have been suggested as a potential solution. The number of CO_2 storage installations has significantly increased since its inception in 2004.

Numerical simulations provide a more effective analysis tool for the geomechanical behavior of complex problems compared with conventional approaches. Due to it being heavily dependent on the available data of geomechanical input, which can vary between carbon dioxide capture and storage (CCS) locales, the numerical technique is much more contextual than empirical methods. Additionally, the simulation results may vary depending on the features of the numerical tools, such as formulation, discretization, problem complexity, and modeling logic. Several high-profile papers[1−4] provide a generic analysis and knowledge gained from previous investigations on the CO_2 injection-storage process and fault reactivation incidents caused by pressure buildup in the reservoir. One such analysis of fault reactivation highlights the low possibility of fault reactivation at deep (1000 m and deeper) formations by shale gas fracturing.[1] Given the enormous storage pressure compared to the hydrostatic pressure, their subsequent numerical analysis of the In Salah CO_2 storage site indicates the probability of caprock breaking and deep fracture opening which can potentially induce microseismicity. The study also refers to multiple cases with considerable seismic events that were seldom capable of causing new flow paths along the thick caprock layer. The numerical simulation is useful in getting a realistic representation of the slip process of faults intersecting storage

Received: January 24, 2024
Revised: July 6, 2024
Accepted: July 10, 2024
Published: July 17, 2024

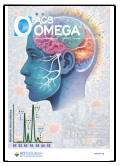

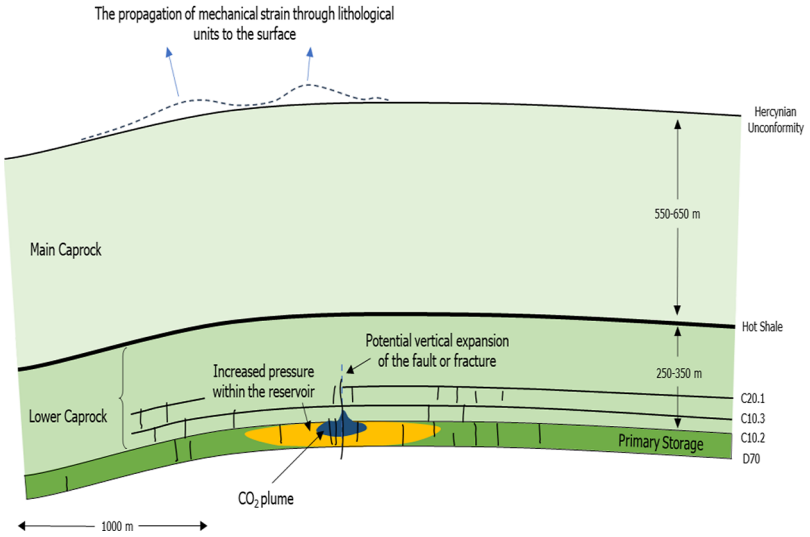

Figure 1. Diagram depicting the primary geomechanical observations surrounding injection well KB-502 at the In Salah CO2 storage site in Algeria.

Table 1. Depth and Thickness Ranges of the Major Domains Proposed in the Past Studies of the In Salah CO_2 Storage Site

past In Salah CO_2 storage numerical investigations	overburden depth range (m)	main caprock depth range (m)	lower caprock depth range (m)	underburden depth range (m)
lessons learned and knowledge transfer[8]	<1000	1000−1600	1600−1900	>1900
inverse modeling of ground surface uplift and pressure[17]	<900	900−1450	1450−1800	>1820
coupled reservoir-geomechanical analysis[18]	<900	900−1450	1450−1800	>1820 or >1900
geomechanical behavior of the reservoir and caprock[20]	<850	850−1550	1550−1800	>1820

sites while studying fault mechanisms. Many researchers studying fault reactivation in CCS sites tend to utilize finite difference, finite volume, finite thickness, and finite element codes for their simulations, emphasizing their effectiveness.[1,4−6] Examining the progression of fault reactivation would be possible by implicitly modeling the temporal influence on the geomechanical behavior of the storage site.

Site-specific and comprehensive studies frequently place a high priority on performing thorough sensitivity analyses to examine the discrepancies between the base case and parametric studies in more detail and depth. The fault sensitivity, for example, can be analyzed by changing solely injection quantities and removing layers except for the fault core.[5] Rutqvist et al.,[1] on the other hand, studied the fault response to the alterations in injection depth, fault dip, slip-weakening parameters, and fracture zone height from the reservoir, which ultimately did result in noticeable deviations from the field observations. Yet, there is a promising potential in investigating fault behavior by changing many other parameters such as effective stress ratio, rock mass properties, and pressure profile. Several studies emphasize the importance of studying effective stress changes in deep geological faults,[1,4,7] as they appear to be highly sensitive to these alterations. Second, the changes in rock mass parameters are also highly likely to cause deviations in slip displacements from the base observations. For example, an incompetent rock mass with weak cohesion and friction angle parameters is expected to trigger fault reactivation and correspondingly intensified surface deformations.

The analysis may further be enhanced by incorporating various aspects and parameters of the CO_2 storing process such as molar fractions,[9,10,12] temperature,[2,9−14] gas density,[9−12] viscosity,[9−14] and saturation.[2,10−14] The investigations also commonly mention the importance of including the permeability and pressure in the reservoir. The pressure amount in the CO_2 storage comes as a limitation on the gas amount being injected since the integrity of the seal caprock and avoidance of fracture or fault reactivations are the main priorities.[11] This is due to the level of sophistication the numerical tools have that analytical methods often lack. As a result, fault reactivation and induced seismicity are key factors in the investigation of geological carbon storage.

2. METHODOLOGY

2.1. In Salah CO_2 Storage Site. To investigate fault reactivation mechanisms in CO_2 storage sites, the In Salah CO_2 storage site, as illustrated in Figure 1, was selected for the numerical simulation, as it appears to be a good candidate site for our numerical study. Previous investigations[8,15−20] were largely concerned with the geomechanical characteristics of the In Salah site and the reasons that might have contributed to this behavior. Significant research has been conducted on various injection wells (KB-501, KB-502, and KB-503) on the site, and the correlation between surface uplift and pressurization was investigated. Table 1 presents a summary of the investigations pertaining to the geological model and the geometry of the storage site.

At a depth of 1880 m below the surface, the main CO_2 reservoir aquifer, which has a thickness of 20−25 m, is located. The formation is characterized by a Carboniferous Tournasian sandstone unit. A massive sandstone and siltstone deposit of comparable thickness is located just above the storage

https://doi.org/10.1021/acsomega.3c08859
ACS Omega 2024, 9, 32513−32524

reservoir, as illustrated in Figure 2. The lower caprock zone between approximately 1550 and 1800 m depth acts as a

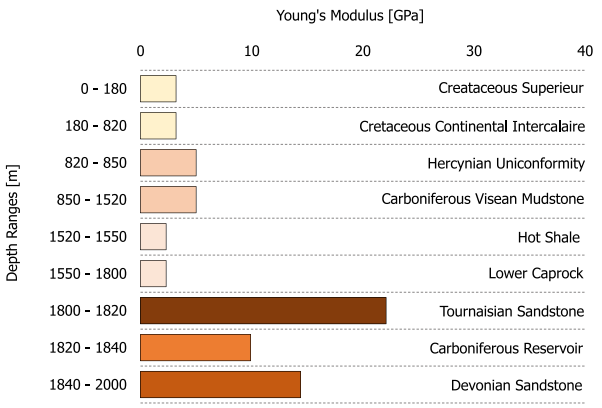

Figure 2. Changes in the rock mass deformation modulus with depth intervals from the stratigraphic columns at well KB-502 at the In Salah site.

sealing unit for the reservoir consisting of silty shale with fractures.[8,20−22] The main caprock includes Carboniferous Visean mudstone, which is interbedded with siltstone and a thin layer of dolomite. The overburden is characterized by a massive 730 m thick Cretaceous Continental Intracalaire comprising unconsolidated sand and Pan-Saharan aquifer at the 170−900 m depth range and Cretaceous superieur (mainly consisting of limestones and silts) at the 0−170 m depth range.

Previous numerical studies of In Salah CO_2 storage have frequently used sophisticated three-dimensional codes such as FLAC3D or TOUGH-FLAC.[17] Due to the complexity of these models and the time-consuming computation, a detailed sensitivity analysis of important geomechanical parameters may appear to be limited. In this study, the 2D finite element code RS2 was employed to conduct a numerical study of fault reactivation mechanisms. It is essential to incorporate rock mass characteristics such as cohesion, friction angle, deformation modulus, Poisson's ratio, and tensile strength when employing codes such as RS2. There is a noticeable lack of sufficient data on these parameters since little geomechanical research has been carried out. Instead, hydrothermal, seismic, and petrophysical studies are in abundance. The lack of sufficient geomechanical investigations is typically justified by the proven effectiveness of the seal caprock during the years of injection and storage.[23] Since no alarming issues with fractures have been observed, the most noticeable aspect of the storage process is the surface uplift, as documented by the InSAR monitoring technologies. The vertical deformations around the injection wells, including KB-502, which is located in the critical area, are interpreted by the InSAR tools. Instead of focusing just on the deformations at the surface level, the numerical simulation findings presented in this study illustrate the geomechanical behavior of rock mass in the areas surrounding the reservoir (e.g., lower caprock, main caprock, and fault zone). However, the data recorded by the GIS tools would allow for the comparison of numerical results with in situ observations.

2.2. Finite Element Modeling. The finite element method was chosen to investigate the geomechanical behavior of the CO_2 storage system at the In Salah storage site. The finite element method (FEM) is a robust numerical tool extensively used in various areas of geotechnical engineering and geomechanics design. Unlike finite discrete modeling (FDM) or any other numerical approach, the FEM comes as an approximation to continuum problems such that a finite number of elements make up the continuum domain of analysis, and a finite number of parameters define their behavior.[24] The modeling itself requires satisfaction of certain boundary (edge) conditions on the dependent variables or their derivatives or, alternatively, a boundary value problem. The solution is achieved through several steps, including mesh setup and initial discretization, which greatly affects the accuracy of the numerical simulation. During the computation, it is expected that equilibrium conditions or a sufficient variational approach will be used to determine the stiffness matrix and the load vector of elements from the postulated displacement model.[25] The nodal displacements are calculated by assembling the stiffness matrices and load vectors for each of the assigned elements. The system of equations is solved simultaneously to determine the equilibrium state of the problem. The equilibrium condition is expressed as

$$K\Delta U = P - F \tag{1}$$

Here, P represents applied loads; F denotes internal forces; and ΔU is the nodal displacement vector. For nonlinear analysis, loads are incrementally applied: $P_{(1)}$, $P_{(2)}$, and so forth. The primary goal is to solve this equilibrium equation iteratively for each load step. For the nth load step, the equation is iteratively solved as

$$K\Delta U_{(i+1)} = P_{(n)} - F_{(i)} \tag{2}$$

This iterative process is illustrated using a nonlinear spring example. Initially, the displacement $U_{(n)}$ is known for the load $P_{(n)}$. The task is to determine the response for the next load increment, $P_{(n+1)}$. The internal force $F_{(0)}$ at equilibrium with $P_{(n)}$ is calculated first. Then, the displacement and recalculation of the internal force are updated. Iterations continue to reduce the load imbalance $P_{(n+1)}-F_{(i)}$ and displacement increments $\Delta U_{(i)}$, converging toward the true solution. To ensure computational efficiency, stopping criteria are used to terminate iterations when results are "sufficiently close." RS2 code provides three convergence criteria, including absolute energy, absolute force, and absolute force and energy. For this simulation, absolute energy is chosen due to convergence being achieved when the relative change in energy between iterations falls below a specified tolerance, which provides consistent results within RS2. Thus, the criteria ensure that the solution is accurate and computationally efficient, making the FEA process robust and reliable.

For this study, the Mohr−Coulomb failure criterion was applied as the material constitutive law for the domain of analysis. It is the predominant failure criterion utilized in the field of geomaterials, especially soils.[26,27] The model incorporates Coulomb's hypothesis, implying a linear relationship between the shear strength on a plane and the normal stress applied to it:

$$\tau = c - \sigma_n \tan \phi \tag{3}$$

where τ is the shear strength, σ_n is the normal stress (tension positive), ϕ is the angle of internal friction, and c is the cohesion. By using the Mohr−Coulomb criterion, it would enable the mechanical response of the material to be characterized by isotropic shear strength (peak and residual) of cohesive-frictional behavior, increasing with the magnitude of stress/confinement in a linear relationship. The Mohr−

https://doi.org/10.1021/acsomega.3c08859
ACS Omega 2024, 9, 32513−32524

Coulomb model in RS2 is an elasto-brittle-plastic material model in general. In the case where the residual values are the same as peak values, the behavior is elasto-perfect-plastic. The elasto-plastic finite element analysis often utilizes Newton's method. An alternative to this is the *initial stiffness method*, where a global stiffness matrix is created at the start of the analysis and remains unchanged throughout the process. This approach lowers computational effort by avoiding the need to reform the stiffness matrix at every iteration, unlike in Newton's method. However, this method requires a larger number of iterations to converge, which may counterbalance the time saved by keeping the stiffness matrix constant. At each iteration, the following equation system is solved:

$$U^i = K^{-1}R^{i-1} \tag{4}$$

Here, K represents the stiffness matrix, R^{i-1} is the residual force from the previous iteration, and ΔU^i is the displacement change for the current iteration. The residual force R^{i-1} is the difference between the external and internal forces during the current iteration. The internal force at iteration i is usually calculated as

$$F^i_{\text{int}} = \int B^T \sigma^i dV \tag{5}$$

where B is the strain−displacement matrix, and σ^i is the stress tensor. The total displacement at the ith iteration is calculated as

$$U^i = U^{i-1} + \Delta U^i \tag{6}$$

The total displacement is, thus, the summation of the displacement at the previous iteration and the displacement calculated using eq 4. The *accelerated initial stiffness method* accelerates the convergence of the initial stiffness method by scaling the iterative displacements using an acceleration parameter, α, for every other iteration. Thus, for the accelerated initial stiffness method, rather than using (6) to calculate the displacement, it is calculated using

$$U^{2i} = U^{2i-1} + \Delta U_e^{2i} \tag{7}$$

$$U^{2i+1} = U^{2i} + \alpha^{2i}\Delta U_e^{2i+1} \tag{8}$$

where α is the acceleration parameter applied for every other iteration. Equations 7 and 8 are alternated for each iteration such that the acceleration parameter is only applied for every other iteration. Ultimately, the parameter of acceleration is computed by the following equation:

$$\alpha^{2i} = \begin{cases} \alpha^{2i-2} + \dfrac{\{\Delta U_e^{2i}\}^T\{\Delta U_e^{2i}\}}{\{\Delta U_e^{2i}\}^T\{\alpha^{2i-2}\Delta U_e^{2i-1}\}} & \text{for } i > 1 \\ 1 \quad \text{for } i = 1 \end{cases} \tag{9}$$

Table 2 provides a summary of the stress analysis criteria employed within the RS2 environment.

2.3. Input Parameters. The rock mass tensile strength, friction angle, cohesion, and mechanical properties are the main material data required as inputs for the RS2 code. Figure 2 shows the change in the rock mass deformation modulus for the In Salah site as a function of depth. Table 3 presents rock mass geomechanical parameters that are compiled from the In Salah database and processed using the RocLab program aimed at determining rock mass design parameters. The data are presented as a function of reservoir depth and used as input in numerical simulations.

Table 2. Stress Analysis Criteria in the RS2 Code

parameters	value
convergence type	absolute energy
initial stiffness acceleration, α	minimum = 0.3; maximum = 3.0
joint tension reduces joint stiffness by a factor of	3.0
tensile failure reduces shear strength to residual	enabled

The sequence of the CO_2 storage process in the Krechba Field, In Salah, includes constantly changing injection rates and pressure levels in the reservoir. The variations in injection rate, pressure, and sequence significantly affect the in situ behavior of the seal caprock and developed fractures. While BHP reflects the total pressure at the bottom of the wellbore, which includes contributions from both the reservoir fluids and any additional pressure exerted by the injection process, and is influenced by factors such as injection rate, volume, and the properties of the reservoir rock, the data in previous comprehensive calculations[17] guides with validating the pressure dynamics. Thus, the dynamics of bottom-hole pressure was taken into consideration for a further quantitative comparative analysis to provide realistic loading data for numerical modeling. The variations in reservoir pressure between 2008 and 2011 are used for further investigation. The bottom-hole pressure data was digitized from the wellhead pressure using T2Well code[17] (assuming 2 MPa standard deviation in the calculated BHP) and then further processed to evaluate the dynamics of the bottom-hole pressure during a period of three consecutive years, from 2005 to August 2008. The injection process for KB-502 was halted between 2007 and 2008 following the detection of CO_2 at the wellhead of a nearby previously drilled appraisal well and was eventually terminated in 2011.[21] Initially, as the injection process began in 2005, BHP and WHP increased sharply, reflecting the pressure needed to overcome reservoir resistance and initiate fluid entry into pore spaces, contributing to capillary and structural trapping. BHP stabilizes despite the inconsistent injection rate between 2006 and mid-2007, potentially denoting the effective residual trapping, as the fluid occupies pore spaces and interacts with the stratigraphic layers. Due to the suspension of injection, the pressure decline continues through late 2007 and 2008, during which fluids remain trapped primarily by residual and structural mechanisms, with the reservoir's pore spaces and structural traps effectively containing the fluid. Table 4 illustrates the major loading steps determined from the pressure history of well KB-502[17] and is used as an input for the numerical analyses.

2.4. Parametric Analysis. In order to investigate the fault reactivation mechanisms, a comprehensive analysis of key geomechanical and geometric parameters was carried out. Table 5 outlines the conducted simulation scenarios, including the benchmark run (Run #1) simulation. In the sensitivity study, one specific parameter of choice was changed keeping the remaining input parameters unchanged. Changes in the effective stress ratio and fault angle described above may result in potential alterations in the storage site displacement field, which may result in fault reactivation. While we consider fault dipping angles to be low (30°), fairly steep (60°), and vertical (90°), we do not contemplate horizontal fractures since the

https://doi.org/10.1021/acsomega.3c08859
ACS Omega 2024, 9, 32513−32524

Table 3. Rock Mass Data Determined for the In Salah Site as a Function of Depth

zones/layers	depth (m)	Young's modulus (GPa)	Poisson's ratio	cohesion (MPa)	friction angle (deg)
overburden	0−800	3	0.25	1.5	22
main caprock	800−1520	5	0.30	5.0	25
lower caprock	1520−1820	15	0.25	8.0	37
underburden	1820−2000	20	0.30	10.5	35

Table 4. Determined Bottom-Hole Pressure Intervals During the Injection Period at Well KB-502

stage	period	duration (months)	pressure (MPa)	pressure factor
1	Mar. 2005−Sept. 2005	6	26	1
2	Sept. 2005−Mar. 2006	6	29	1.11
3	Mar. 2006−Sept. 2006	6	31	1.19
4	Sept. 2006−Mar. 2007	6	32	1.23
5	Mar. 2007−Jul. 2007	4	28	1.08
6	Jul. 2007−Oct. 2007	3	23	0.88
7	Oct. 2007−Feb. 2008	4	21	0.81

Table 5. Summary of Parametric Study Conducted for the In Salah Site

runs	fault dipping angle (deg)	horizontal to vertical stress ratio, k	small vertical fractures above reservoir
1	60	2	0
2	60	1	0
3	60	0.5	0
4	60	3	0
5	30	2	0
6	60	2	3
7	90	2	0

presence of major horizontal faults in the vicinity of the storage site remains unclear and not well-documented. The occurrence of mainly vertical fractures around injection well KB-502 is illustrated in Figure 1. Changing it to a low-angle fault (30°) is hence used to evaluate the sensitivity of the model by analyzing the mechanical response (surface deformation). Besides the traditional investigations of the fault dipping angle and stress ratio influence, it is believed that the consideration of vertical artificial fractures in the seal unit (lower caprock) of the reservoir may further demonstrate the deformation mechanisms observed at the storage site. Given the excessive pore pressure, it is conceivable that the fractures cause the seal rock's integrity to deteriorate, which leads to carbon dioxide leakage from the storage. In a separate analysis, the caprock above the storage zone was accomplished with a set of artificial vertical discontinuities/fractures that were 20 m long and oriented vertically.

2.5. Numerical Simulation Strategy. The two-dimensional finite element code (RS2) was employed to model the In Salah storage site in a simplified manner and simulate the effects of probable fault reactivation as a function of the change in reservoir pressure. A field-scale 2D modeling of the storage site was carried out, and the displacement and stress fields of the entire storage site were determined. The strategy and workflow of the numerical simulation and parametric study is detailed in Figure 3.

The geometry employed in the model (Figures 4 and 5), with some approximation and modification, is consistent with those investigated by geotechnical surveys and log well analysis for the In Salah CO_2 storage site. The data published in previous geomechanical and geological investigations were used to compile the physical and mechanical characteristics of the rock masses at the In Salah storage site (Table 3). These properties were used as input for the conducted numerical modeling analyses. In order to further analyze the changes in the storage site displacement field, major components of displacement and stress were monitored at key points in particular in the vicinity of the fault plane. Accordingly, 30 monitoring points were placed at critical points within the model, as illustrated in Figure 4. The monitoring point numbers 11−30 are located to look into the geomechanical behavior of the fault zone. Therefore, two identical sets of control points are placed on both the left-hand and right-hand sides of the fault. The time query points from 0 to 10, on the other hand, represent a vertical set of monitoring points above the reservoir, which provides additional detailed data for the comparison of geomechanical results at different zones. The analysis domain was discretized using linear, uniform-sized, three-node triangular elements. As shown in Figure 5, the region of interest was discretized using 20,000 total elements.

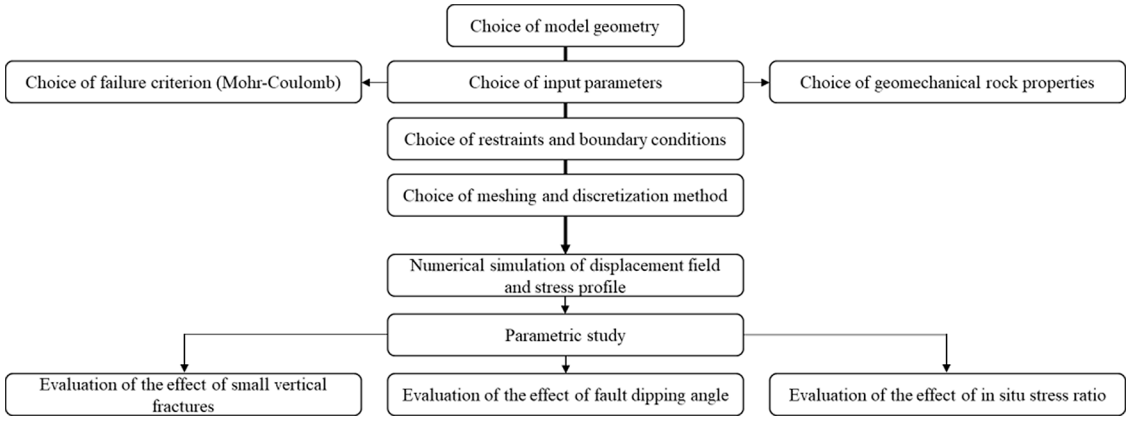

Figure 3. Methodology was used to conduct numerical simulation.

https://doi.org/10.1021/acsomega.3c08859
ACS Omega 2024, 9, 32513−32524

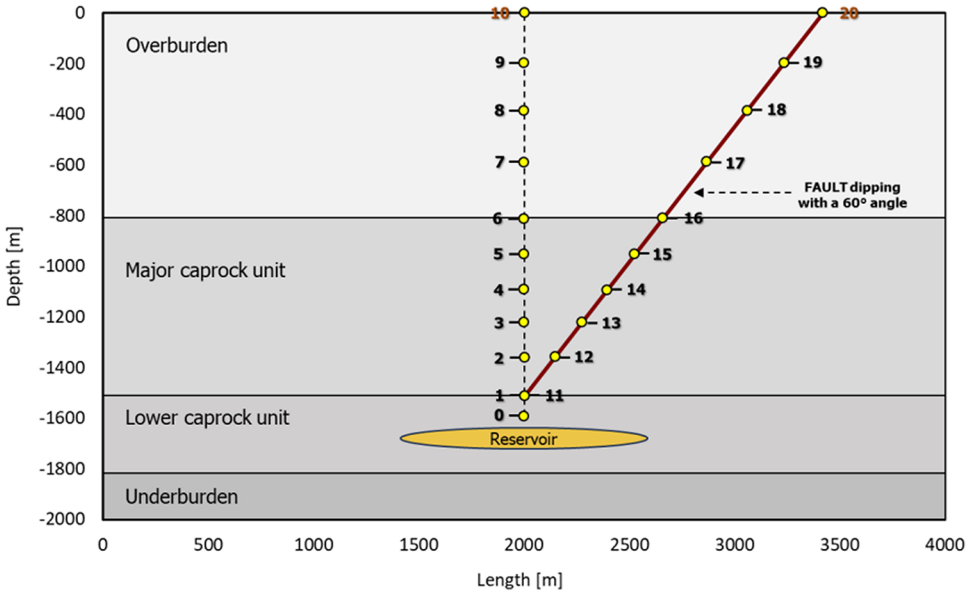

Figure 4. Illustration of the modeling domain geometry indicating the location of monitoring points.

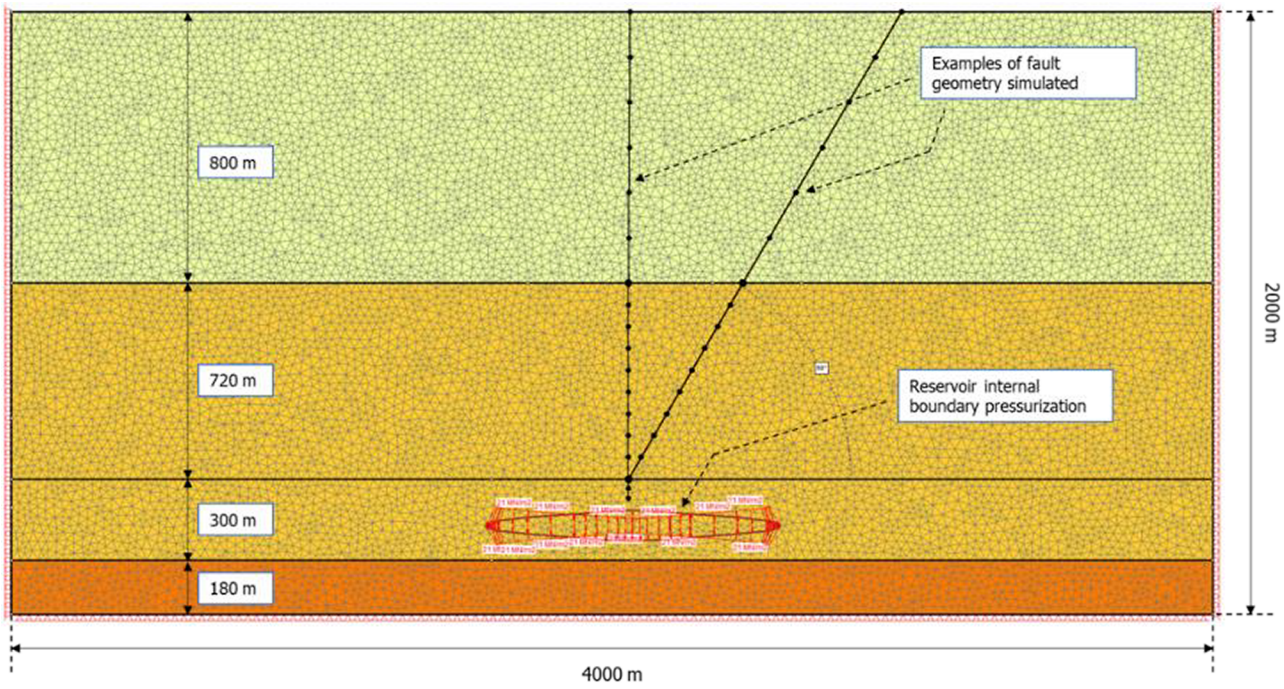

Figure 5. View of the RS2 model of the In Salah storage site and main lithological units at injection well KB-502.

3. RESULTS AND DISCUSSION

To investigate the fault reactivation mechanisms, a base run analysis was carried out using the parameters summarized in Tables 3 and 4. Following the base case scenario investigation, a parametric study outlined in Table 5 was conducted. The obtained results are presented in the following sections.

3.1. Numerical Simulation Results. The storage site stress field was computed for the base run scenario, and a summary of results is presented in Figure 6. Assuming a stress ratio of 2 and no pressurization (prior to CO_2 injection), Figure 6a,b shows the distribution of horizontal and vertical stress fields, respectively. Furthermore, the distributions of shear and mean stress are illustrated in Figure 6c,d, respectively. As there is no evidence of the fault reactivating before pressurization, only a small amount of slip on fault and a good seal caprock integrity are predicted. The level of pressure buildup in the storage is the main cause of caprock deformation and rock mass geomechanical response. In the base run scenario, a linear variation of all stress components is observed.

Figures 7 and 8 illustrate changes in horizontal and vertical displacements measured at the monitoring points located along the fault line as a function of the storage site pressurization. The deformation at the measuring points along the 60° dipping angle fault suggests that the pressurization cycle immediately affects the geomechanical behavior of the reservoir host rock. The pressurization stages 3 and 4 (31 and 32 MPa, respectively) resulted in maximum horizontal and

https://doi.org/10.1021/acsomega.3c08859
ACS Omega 2024, 9, 32513−32524

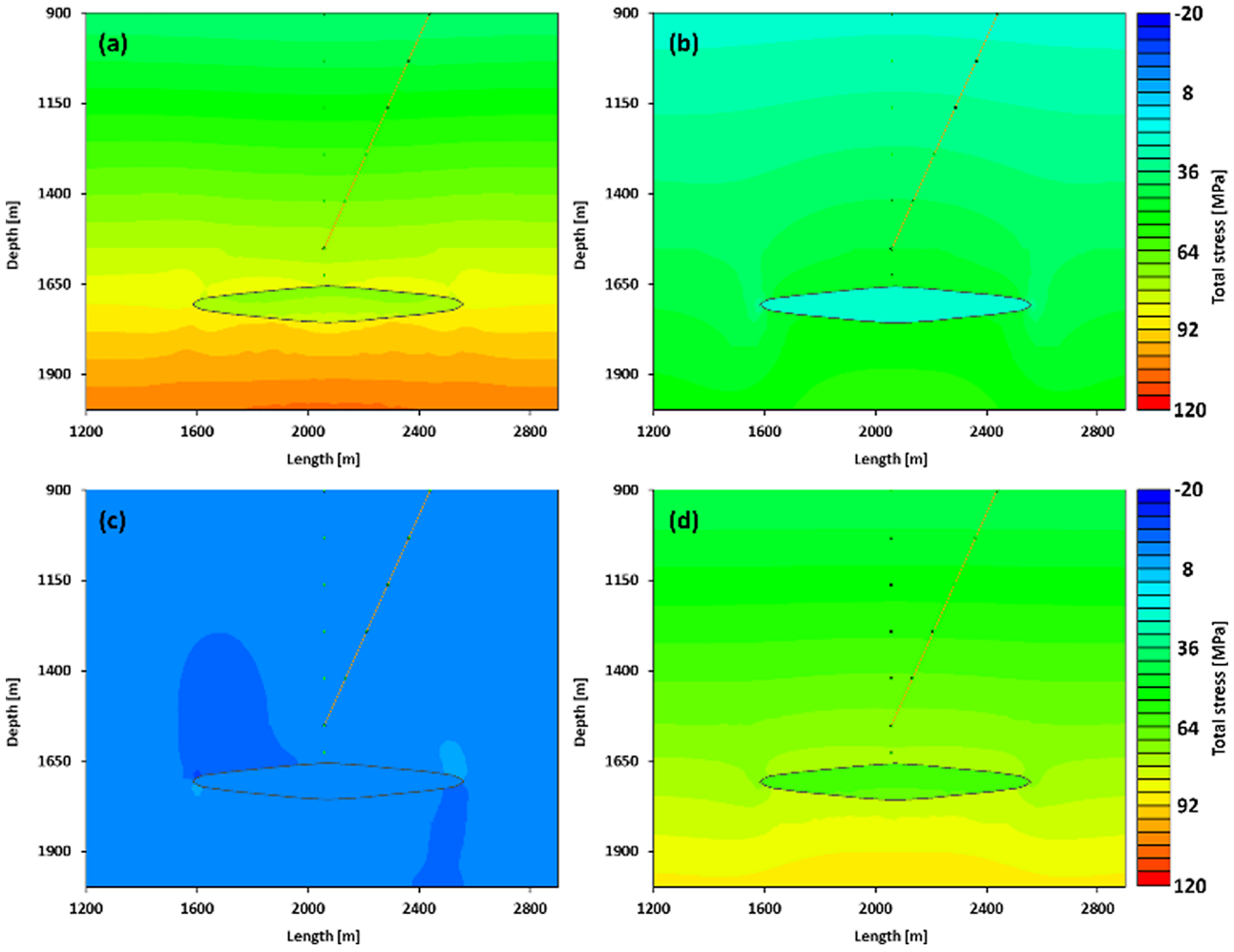

Figure 6. In situ stress distribution around the fault-reservoir zone: (a) horizontal stress (σ_{xx}), (b) vertical stress (σ_{yy}), (c) shear stress (Σ_{XY}), and (d) mean stress.

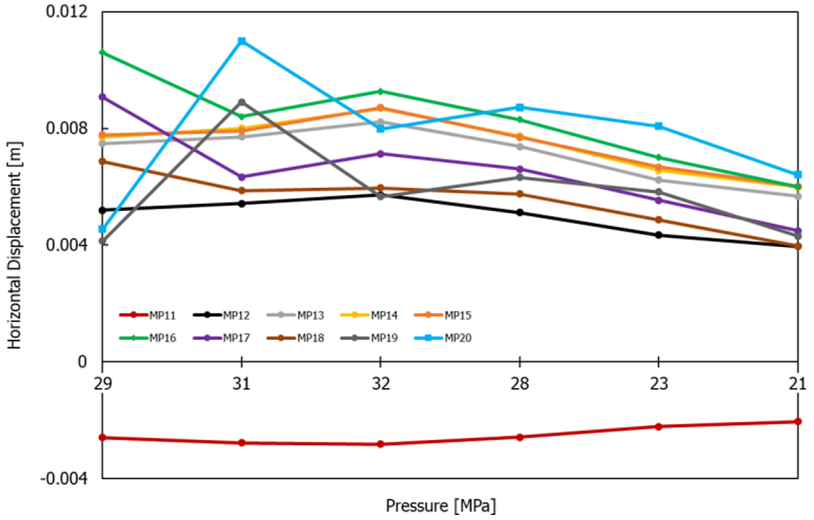

Figure 7. History of the change in horizontal displacement at the selected monitoring points located along the 60° dipping fault.

vertical displacements along the fault plane. The monitoring point no. 20, which is located at the ground surface level, showed the highest horizontal displacement of 0.011 m. The recorded caprock vertical displacement at the selected monitoring points, on the contrary, demonstrates a clear trend of decreasing displacements with increased elevation of the monitoring points (Figure 8). This demonstrates that the caprock is subjected to a higher magnitude of vertical displacement in the top portion of the reservoir, where the pressurization may act as a driving factor of the rock

https://doi.org/10.1021/acsomega.3c08859
ACS Omega 2024, 9, 32513−32524

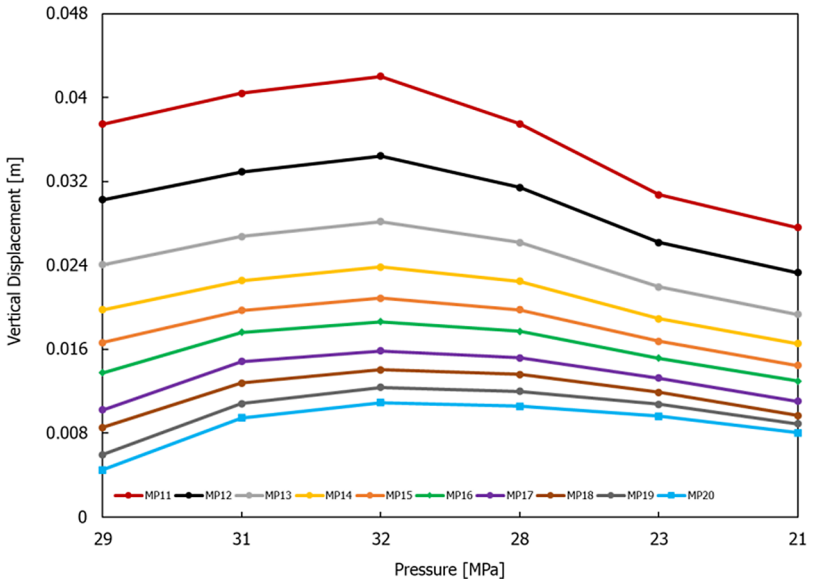

Figure 8. History of the change in vertical displacement at the selected monitoring points along the 60° dipping fault.

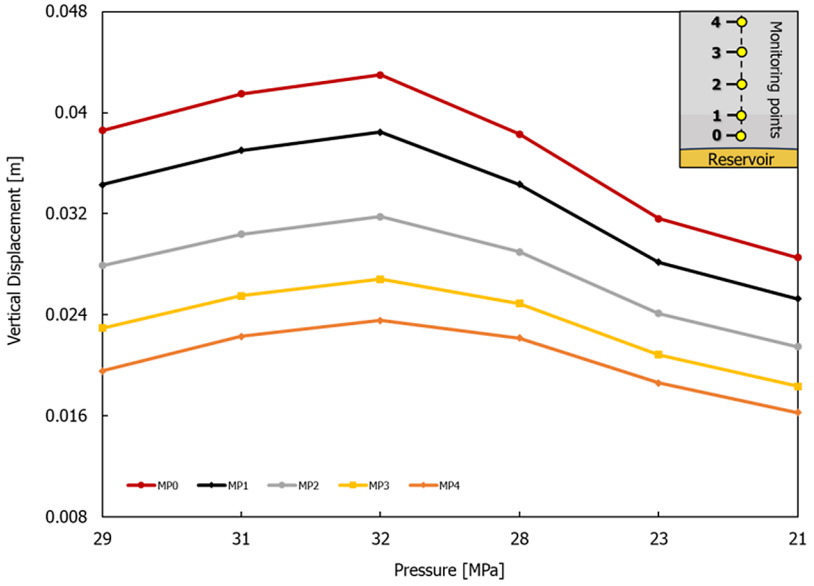

Figure 9. History of the change in vertical displacement in the top portion of the reservoir (monitoring points 0−4) along a vertical line within the caprock and on top of the storage site.

deformation. This is more evident as the vertical displacements increase in response to gradually rising pressure from 26 to 32 MPa. Ultimately, all selected monitoring points show maximum displacements at pressurization stage 3, which has the highest-pressure cycle of 32 MPa. Moreover, the change in vertical displacement field recorded at the top portion of the reservoir (Figure 9) demonstrates a similar trend observed at the selected monitoring points. The maximum vertical displacement that was recorded at the monitoring point MP0 is about 0.042 m.

The selected monitoring points located on the ground surface enable a comparison of numerical data with actual observations and monitoring. The monitoring points nos. 10, 20, and 30 demonstrate the ground surface uplift during the reservoir pressurization phases. Based on the numerical data recorded at these points, an average vertical displacement of about 0.026 m was determined for the ground surface level. Figure 9 displays that the determined vertical uplift profile at monitoring point 20 (surface level) is in good agreement with the recorded past InSAR surface monitoring readings of 0.005−0.020 m. The dynamics of the vertical deformation at the surface level showcases a gradual ground uplift through 2005 into early 2007 (before the injection suspension), which is strongly influenced by the commencement of the injection and further steady increase. As the postsuspension period (between mid-2007 and 2008 and after) approaches, the pressure dissipates, and the magnitude of the uplift declines accordingly, marking the slow subsidence of the ground after 2008 and until the ultimate discontinuance of injection in 2011. Figure 7 also reveals that the overburden layer (in the depth range of 0−900 m; monitoring points 16−20) is more highly impacted by the changes in the pressurization in contrast to the main caprock (in the depth range of 900−1550 m; monitoring points 11−15).

https://doi.org/10.1021/acsomega.3c08859
ACS Omega 2024, 9, 32513−32524

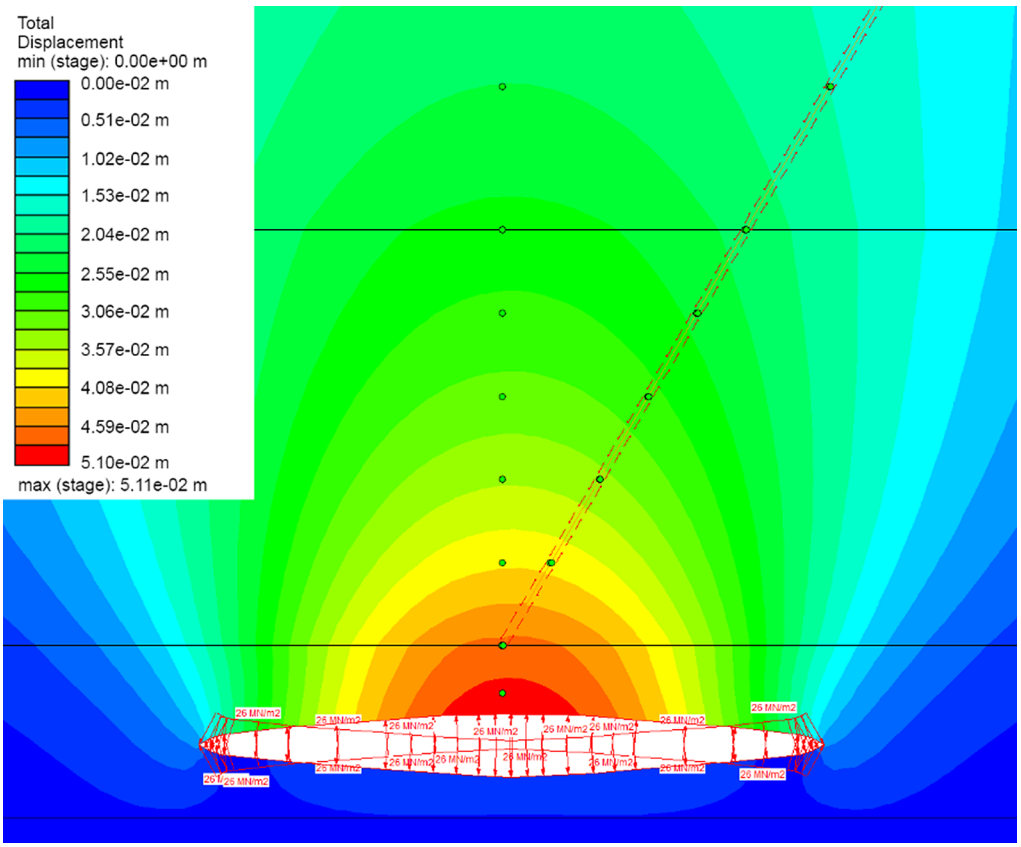

Figure 10. Geomechanical response of the model to the initial pressurization (26 MPa) of the reservoir.

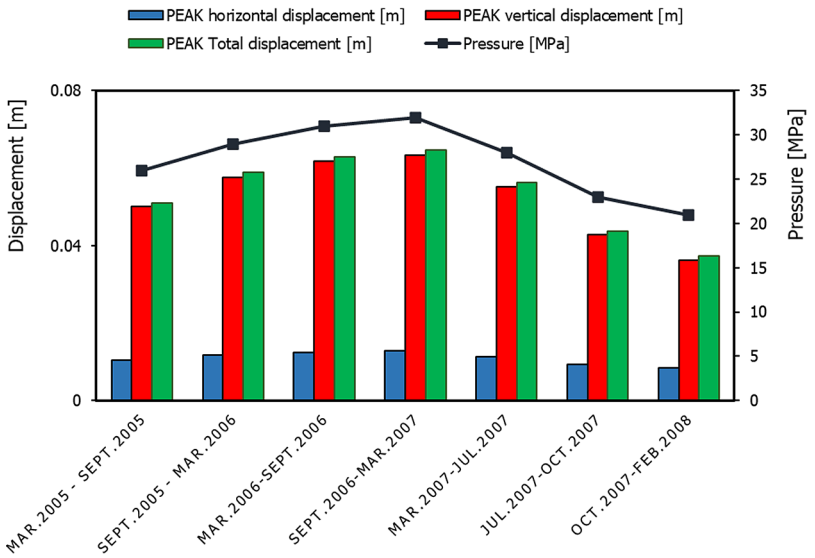

Figure 11. History of simulated peak displacement magnitudes at monitoring points 11−20 correlated with the pressurization cycle.

The maximum vertical displacement during the first pressurization phase (26 MPa) in the gas reservoir was determined as 0.034 m, after which the deformation would become larger due to the increase in pressure. Because the stiff sandstone layer and the seal rock underwent horizontal deformation as well, the combined displacement of these units peaked at 0.051 m (Figure 10). The approximately 20 m thick and 50 m long zone of the seal unit at the upper portion of the reservoir sustained the maximum deformation due to the reservoir geometry and pressure acting on the lower caprock. Conversely, there was very little deformation along the outer boundaries of the storage. However, the overall results of the first pressurization demonstrate good integrity of the seal unit, allowing only small displacements of up to 51 mm. From the point of view of preventing carbon dioxide leakage, the simulated scenario is regarded as fairly stable and safe.

Considering the influence of the pressure level on the deformation of the storage zone host rock, Figure 11 illustrates a rather straightforward relationship between the injection pressure level and the reservoir's horizontal and vertical

https://doi.org/10.1021/acsomega.3c08859
ACS Omega 2024, 9, 32513−32524

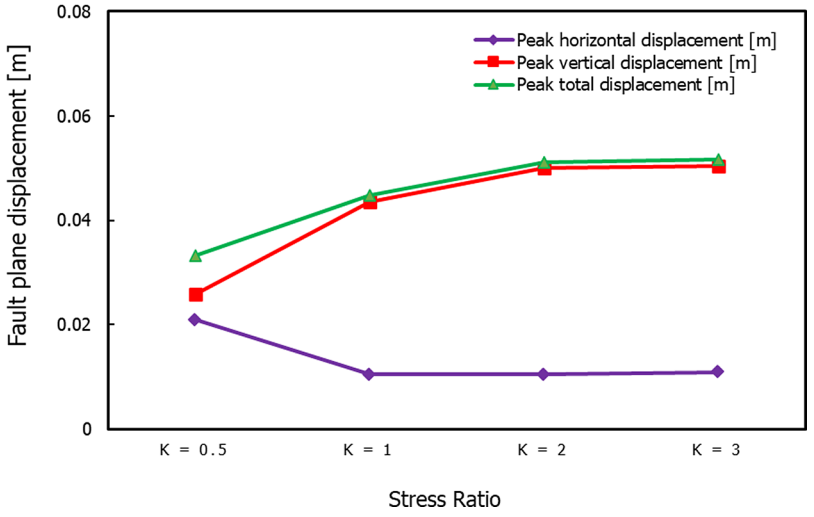

Figure 12. Sensitivity analysis results of variation of fault plane displacement as a function of changes in the stress ratio.

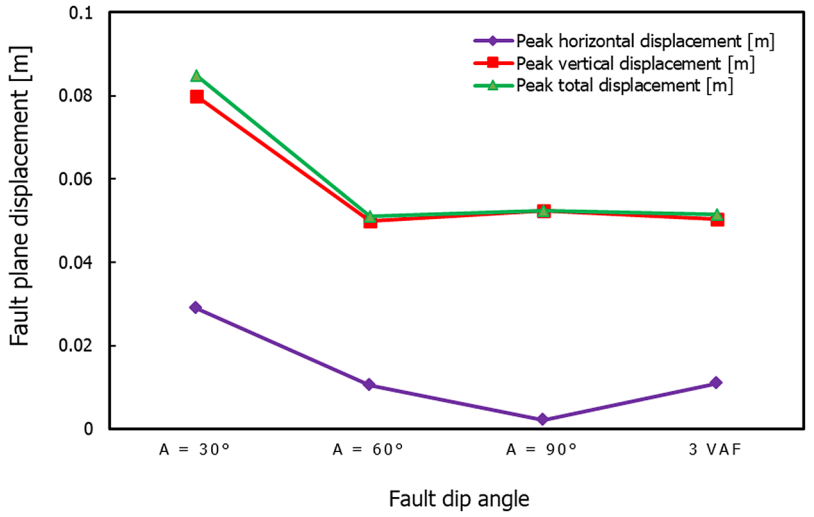

Figure 13. Sensitivity analysis results of variation of fault plane displacement as a function of change in the fault dipping angle.

displacement fields. Taking into account the history of sequential injection pressure, an increase in pressure from 26 to 32 MPa caused a proportionate deformation of the host rock. Therefore, if we apply similar reasoning, a drop in pressure to 21 MPa directly led to a decrease in both horizontal and vertical displacements. Considering the suspension of the CO_2 injection in mid-2007 and ultimate termination in 2011, the pressure level is assumed to continue to decrease gradually. Additionally, pressure readings are available up to mid-2008, and the pressure data after mid-2008 remain unclear. In light of this, the predicted displacement behavior shown in Figure 11 might imply that surface and fault plane deformation levels keep declining in accordance with the reduced pressurization.

3.2. Sensitivity Analysis. A sensitivity analysis of the effects of the horizontal-to-vertical stress (k) ratio was conducted because in situ stress is one of the most important boundary conditions of the problem. Major displacement components along the fault plane (monitoring points 11−20) were computed by using different stress ratios as boundary conditions in separate runs. The obtained results demonstrate how highly sensitive the movement is to the stress ratio along the fault plane. As demonstrated in Figure 12, the fault displacement becomes less sensitive at stress ratios of 3 and above. Nevertheless, the modeling results indicate greater sensitivity and more noticeable changes in the global fault plane displacement for stress ratios of less than 2 (the base run scenario). A significant decrease in the vertical displacement of the fault is seen at a stress ratio of 0.5, and for this particular case, a vertical displacement of 0.025 m is determined. In the present case, the total displacement of the fault plane is 0.033 m. Conversely, the horizontal displacement of the fault plane demonstrates the opposite trend. The fault plane's maximum horizontal displacement is calculated at a stress ratio of 0.5, and as the stress ratio increases, the fault plane's horizontal displacement decreases. The monitoring point number 11 is where the displacement component maximum values are determined. This point's proximity to the highly stressed zone above the reservoir and below the fault start location could again justify the maximum displacement in this area. The base run scenario, where the fault plane was dipping at a 60° angle, and only the stress ratio changed, produced the results shown in Figure 12; all other input parameters were kept unchanged. The results obtained reveal that, despite higher stress ratios of 3 and higher, the fault's dipping angle prevents large fault movements.

https://doi.org/10.1021/acsomega.3c08859
ACS Omega 2024, 9, 32513−32524

Figure 13 illustrates the findings of a second set of analyses that examined the effects of the fault dipping angle on fault plane displacement. When comparing the reservoir displacement field to the base run findings, this analysis did not reveal any significant variations. High horizontal stress fields and the high caprock physical integrity are two important reasons for the insignificant influence of vertical artificial cracks considered within the seal unit. The compiled rock mass characteristics of the Salah site, which characterize the caprock, are good enough to withstand significant deformation, thus leading to lower displacements. In this case, the three simulated artificial fractures, each measuring 20 m in length and 90° angle outlined in Table 5, hardly affect the integrity in any way. Given the limited availability of the structural and geomechanical data (the mechanical and strength properties of the rock) for the In Salah storage site, this type of observation is extremely important for the caprock integrity of the In Salah site. Therefore, further variations and uncertainties in the discontinuity/fault configurations and geotechnical domain properties of the caprock could have a substantial impact on the reservoir displacement field, necessitating additional analytical and parametric studies of important geomechanical parameters.

4. CONCLUSIONS

This study included further parametric and sensitivity studies in addition to two-dimensional finite element modeling of fault reactivation processes in the context of CO_2 storage. The In Salah CO_2 storage site was simulated within the RS2 code environment using a 4 km wide and 2 km deep model that included the key domains and formations (underburden, main caprock, lower caprock, and overburden). A thorough numerical analysis considering problem boundary conditions, geological configurations, and important caprock properties was carried out. The following summarizes the main numerical findings, which are in agreement with field observations:

- Only a slight surface uplift (0.015−0.020 m) is observed in the context of base pressurization in the reservoir (26 MPa) and the storage site stress analysis utilizing the parameters obtained from the original log well data. It is primarily assumed that the uplift measured in the injection area is induced by the pressure buildup. The extent of the vertical deformation accordingly became less pronounced as the injection process halted in mid-2007. The surface-level displacements simulated for late 2008 also agree with published results from earlier research including InSAR data accurate for 2009. The peak vertical deformations at the lower caprock layer (0.05 m) have a reduced likelihood of creating any deep fractures, starting new leakage path flows, or endangering the caprock's structural integrity.
- Variations in the in situ stress ratio at a fixed fault dip angle (60°) and unaltered mechanical input had a mild to moderate effect on the geomechanical behavior of the analysis domain. In contrast to the base run scenario, where a stress ratio of 2.0 was taken into consideration, a minimum reference stress ratio of 0.5 resulted in a nearly 50 percent drop in the displacements.
- The parametric study underscores the pronounced influence of fault dip angles, particularly under conditions of elevated stress ratios favoring horizontal in situ stress. At a dip angle of 30°, faults pose heightened risks to reservoir and seal integrity compared to steeper dips. The main reason for this is the high ratio of horizontal stress leading to higher shear stress compared to the frictional resistance on the fault plane at such a low dip angle. The caprock underwent approximately twice as much deformation with the fault dipping at 30° compared to the 60° dip angle. Thus, angles exceeding 45° generally ensure stability (considering k = 2.0), whereas shallower dips may induce instability and fault reactivation.

The caprock integrity investigations would benefit substantially from extensive field measurements and geomechanical data, even though the conclusions are consistent with previous studies of the In Salah CO_2 storage site that employed a similar numerical approach. Consequently, the need for extensive in situ and field studies to measure the rock properties more accurately is necessary. Material properties could be overstated or underestimated in numerical research if this crucial component is overlooked. For CO_2 storage projects, it is also essential to choose a suitable reservoir and seal rock with strong integrity resistant to potential deformations, fault reactivation influence, and microseismic activity. The future studies related to fault reactivation in the context of subterranean CO_2 storage will be conducted using more complex and advanced 3D numerical tools (e.g., 3DEC). These tools will accurately represent complex subsurface geometry, capture spatial variations in stress and pressure, predict fault behavior more realistically, consider possible out-of-plane leakage scenarios and interactions among multiple faults, and enhance risk assessment capabilities, which can ultimately help understand more potential fault reactivation scenarios and mechanisms in CO_2 storage.

AUTHOR INFORMATION

Corresponding Author

Ali Mortazavi − *School of Mining & Geosciences, Nazarbayev University, Nur-Sultan 010000, Kazakhstan;* orcid.org/0009-0008-0835-7326; Phone: +7(7172)694894; Email: ali.mortazavi@nu.edu.kz

Author

Torekeldi Maratov − *School of Mining & Geosciences, Nazarbayev University, Nur-Sultan 010000, Kazakhstan*

Complete contact information is available at: https://pubs.acs.org/10.1021/acsomega.3c08859

Notes

The authors declare no competing financial interest.

ACKNOWLEDGMENTS

The authors gratefully acknowledge the funding provided by Nazarbayev University as part of the FDCRG 2023−2025 (Grant No. 55431188) research project and the funding provided by Chevron/Nazarbayev University Research Collaboration Program as part of the FY2022-Chevron/NU RCP research project.

REFERENCES

(1) Rutqvist, J.; Rinaldi, A. P.; Cappa, F.; Moridis, G. J. Modeling of fault reactivation and seismicity by injection directly into a fault zone associated with hydraulic fracturing of shale-gas reservoirs. *J. Pet. Sci. Eng.* **2015**, *127*, 377−386.

https://doi.org/10.1021/acsomega.3c08859
ACS Omega 2024, 9, 32513−32524

(2) Rinaldi, A. P., Rutqvist, J., Finsterle, S., Liu, H. *Forward and Inverse Modeling of Ground Surface Uplift at In Salah*, ResearchGate: Algeria, 2014; https://www.researchgate.net/publication/262875508.
(3) Lyu, X.; Voskov, D.; Rossen, W. Numerical investigations of foam-assisted CO2 storage in saline aquifers. *International Journal of Greenhouse Gas Control* **2021**, *108*, No. 103314.
(4) Vilarrasa, V.; Makhnenko, R. Y.; Laloui, L. Potential for fault reactivation due to CO2 injection in a Semi-Closed saline aquifer. *Energy Procedia* **2017**, *114*, 3282−3290.
(5) Yoon, S.; Lee, H.; Kim, J. The modeling of fault reactivation, slip, and induced seismicity for geological CO2 storage at a pilot-scale site in the Janggi Basin, South Korea. *International Journal of Rock Mechanics and Mining Sciences* **2023**, *170*, No. 105441.
(6) Preisig, M.; Prevost, J. H. Coupled multi-phase thermo-poromechanical effects. Case study: CO2 injection at In Salah, Algeria. *International Journal of Greenhouse Gas Control* **2011**, *5* (4), 1055−1064.
(7) Kanin, E.; Garagash, I.; Boronin, S.; Garagash, D. I.; Afanasyev, A.; Osiptsov, A.; Zhigulskiy, S.; Penigin, A. *Modelling of Tectonic Fault reactivation During CO2 Sequestration in a Saline Aquifer*. In Sixth International Conference on Fault and Top Seals, 2022, .
(8) Ringrose, P.; Mathieson, A.; Wright, I.; Selama, F.; Hansen, O.; Bissell, R. C.; Saoula, N.; Midgley, J. The In Salah CO2 Storage Site: Lessons Learned and Knowledge Transfer. *Energy Procedia* **2013**, *37*, 6226−6236.
(9) Li, C.; Xu, Z. Numerical Modeling and Investigation of Fault-Induced Water Inrush Hazard under Different Mining Advancing Directions. *Mathematics* **2022**, *10* (9), 1561.
(10) Urych, T.; Chećko, J.; Magdziarczyk, M.; Smoliński, A. Numerical simulations of carbon dioxide storage in selected geological structures in North-Western Poland *Front. Energy Res.* 2022, *10*, DOI: 10.3389/fenrg.2022.827794.
(11) Pomar-Castromonte, R.; Ingol-Blanco, E.; Santos, J.; Santa-Cruz, S. Analytical and numerical modeling for the assessment of CO2 storage in the Pariñas geological formation - Talara, Peru. *International Journal of Greenhouse Gas Control* **2021**, *110*, No. 103446.
(12) Bandilla, K. W.; Celia, M. A.; Leister, E. Impact of Model Complexity on CO2 plume modeling at Sleipner. *Energy Procedia* **2014**, *63*, 3405−3415.
(13) Abbaszadeh, M.; Shariatipour, S. M.; Ifelebuegu, A. O. The influence of temperature on wettability alteration during CO2 storage in saline aquifers. *International Journal of Greenhouse Gas Control* **2020**, *99*, No. 103101.
(14) Nilsen, H. M.; Krogstad, S.; Andersen, O.; Allen, R.; Lie, K. Using Sensitivities and Vertical-equilibrium Models for Parameter Estimation of CO2 Injection Models with Application to Sleipner Data. *Energy Procedia* **2017**, *114*, 3476−3495.
(15) Ringrose, P.; Atbi, M.; Mason, D.; Espinassous, M.; Myhrer, O.; Iding, M.; Mathieson, A.; Wright, I. Plume development around well KB-502 at the In Salah CO2 storage site. *First Break* **2009**, *27* (1), 85−89.
(16) Ringrose, P.; Roberts, D. D.; Gibson-Poole, C.; Bond, C. E.; Wightman, R. H.; Taylor, M. P.; Raikes, S.; Iding, M.; Østmo, S. Characterisation of the Krechba CO2 storage site: Critical elements controlling injection performance. *Energy Procedia* **2011**, *4*, 4672−4679.
(17) Rinaldi, A. P.; Rutqvist, J.; Finsterle, S.; Liu, H. Inverse modeling of ground surface uplift and pressure with iTOUGH-PEST and TOUGH-FLAC: The case of CO2 injection at In Salah, Algeria. *Computers & Geosciences* **2017**, *108*, 98−109.
(18) Rutqvist, J.; Vasco, D. W.; Myer, L. R. Coupled reservoir-geomechanical analysis of CO2 injection and ground deformations at In Salah, Algeria. *International Journal of Greenhouse Gas Control* **2010**, *4* (2), 225−230.
(19) Gemmer, L., Hansen, O., Iding, M., Ringrose, S. L. A. P. *Geomechanical Response to CO2 Injection at Krechba, InSalah, Algeria*. In 1st Sustainable Earth Sciences Conference and Exhibition (SES2011), 2011 .
(20) White, J. A.; Chiaramonte, L.; Ezzedine, S.; Foxall, W.; Hao, Y.; Ramirez, A.; McNab, W. W. Geomechanical behavior of the reservoir and caprock system at the In Salah CO $_2$ storage site. *Proc. Natl. Acad. Sci. U. S. A.* **2014**, *111* (24), 8747−8752.
(21) Mathieson, A.; Midgely, J.; Wright, I. A.; Saoula, N.; Ringrose, P. In Salah CO2 Storage JIP: CO2 sequestration monitoring and verification technologies applied at Krechba, Algeria. *Energy Procedia* **2011**, *4*, 3596−3603.
(22) Durucan, Ş.; Shi, J.; Sınayuç, Ç.; Korre, A. In Salah CO2 storage JIP: Carbon dioxide plume extension around KB-502 well−New insights into reservoir behaviour at the In Salah storage site. *Energy Procedia* **2011**, *4*, 3379−3385.
(23) Armitage, P. J.; Faulkner, D. R.; Worden, R. H.; Aplin, A. E.; Butcher, A.; Iliffe, J. Experimental measurement of, and controls on, permeability and permeability anisotropy of caprocks from the CO2 storage site at the Krechba Field, Algeria. *J. Geophys. Res.* **2011**, *116* (B12), No. B12208, DOI: 10.1029/2011JB008385.
(24) Zienkiewicz, O. C., Taylor, R. T., Fox, D. *The Finite Element Method for Solid and Structural Mechanics*. In Elsevier eBooks, 2014 .
(25) Rao, S. S. *The Finite Element Method in Engineering*. Elsevier eBooks, 2018, .
(26) Owen, D. R. J., Hinton, E. *Finite Elements in Plasticity*, 1980 https://openlibrary.org/books/OL13954022M/Finite_elements_in_plasticity
(27) Pietruszczak, S. *Fundamentals of Plasticity in Geomechanics*, 2010 http://ci.nii.ac.jp/ncid/BB04185022.

https://doi.org/10.1021/acsomega.3c08859
ACS Omega 2024, 9, 32513−32524